

Interpretation of the Underground Muon Charge Ratio

P. A. Schreiner^{a,b}, J. Reichenbacher^{a,1}, M. C. Goodman^a

^a*High Energy Physics Division, Argonne National Laboratory, 9700 S. Cass Ave.
Argonne, IL 60439, USA*

^b*Department of Physics, Benedictine University, 5700 College Road, Lisle, IL 60532,
USA*

Abstract

The MINOS experiment has observed a rise in the underground muon charge ratio $r_\mu = \mu^+/\mu^-$. This ratio can be related to the atmospheric production ratios of π^+/π^- and K^+/K^- . Our analysis indicates that the relevant variable for studying the charge ratio is $E_\mu^{surface} \cos \theta$, rather than $E_\mu^{surface}$. We compare a simple energy dependent parameterization of the rise in the charge ratio with more detailed previously published Monte Carlo calculations. We also estimate the size of two previously neglected effects in this context: the charge sign dependency of the dE/dx in rock, and the energy dependence of heavy primaries on the K^+/K^- ratio.

Key words: Underground Cosmic Ray Muons, Muon Charge Ratio, Meson Charge Ratio

PACS: 13.85.Tp, 13.85.Ni

1. Importance of Charge Ratio Measurements

Atmospheric muons come dominantly from the decay of π s and K s produced in hadronic showers when cosmic rays interact in the earth's atmosphere. These muons have been studied with energies ranging from hundreds of MeV to well over a TeV. A quantitative understanding of cosmic ray muons has value for a number of diverse topics, from atmospheric neutrinos to the chemical composition of the highest energy cosmic rays. The charge ratio of

¹Now at: The Department of Physics and Astronomy, Box 870324, University of Alabama, Tuscaloosa, Alabama 35487 USA

cosmic ray muons has been previously measured over three orders of magnitude in energy. Recently the MINOS experiment[1, 2] presented data that for the first time showed a rise in the measured charge ratio

$$r_\mu \equiv \frac{N^{\mu+}}{N^{\mu-}} \quad (1)$$

from previous measurements at high values of E_μ or more specifically, high values of $E_\mu^{surface} \cos \theta$.

In this paper, we discuss some of the issues involved in the measurement and interpretation of the muon charge ratio. In particular, we develop a simplified model where the rise in the charge ratio can be understood from the properties of π and K mesons, and the observation of the rise can be used to determine the π^+/π^- and K^+/K^- ratios. We also address several other issues related to the measurement of the charge ratio, including the role of muon energy loss, a detector's Maximum Detectable Momentum (MDM), and the effect of possible differences in the spectral index of cosmic ray Hydrogen and Helium on the interpretation.

Since the primary cosmic rays are mostly positively charged protons, more secondary π^+ are expected than π^- . The quark content of the protons and of the atmosphere has been used to estimate the π^+/π^- ratio to be near 1.27 [3]. The charge ratio for kaons is even higher due to the phenomenon of associated production. Strange particle production starts with the creation of an s quark and an \bar{s} quark. An s quark which ends up in a nucleus is associated with an \bar{s} quark in a $K^+(\bar{s}u)$. The \bar{s} quark will not be in a baryon. There is also K^+K^- pair production. Phase space favors hadronic production of $K^+\Lambda$ over K^+K^- pairs at all energies, so large K^+/K^- ratios are expected.

A standard parametrization of the atmospheric muon energy spectrum is given by Gaisser[4]:

$$\frac{dN_\mu}{dE_\mu} = \frac{0.14E_\mu^{-2.7}}{\text{cm}^2 \text{ s sr GeV}} \times \left\{ \frac{1}{1 + \frac{1.1E_\mu \cos \theta}{\epsilon_\pi}} + \frac{\eta}{1 + \frac{1.1E_\mu \cos \theta}{\epsilon_K}} \right\} \quad (2)$$

The two terms inside the curly bracket give the contributions from charged pions and kaons. For the hadron mass (m_i) and lifetime (τ_i), and the atmospheric scale height ($h \sim 6.4$ km), the values of $\epsilon_i = m_i ch/\tau_i$ are the energies where the probability of meson interaction in the atmosphere and decay are equal: $\epsilon_\pi=115$ GeV and $\epsilon_K= 850$ GeV[5]. The zenith angle is denoted by

θ . In those experiments with a flat overburden, the largest muon intensity is at $\cos(\theta) = 1$. Reference [4] gives $\eta = 0.054$, which sets the relative contribution to the muon flux from π and K decay. The parameter η depends upon the π/K ratio, branching ratios, and kinematic factors which arise due to differences between the π and K masses.

The ratio between the two terms in Equation 2 quantifies the relative contribution to the muon flux from muons due to π and K decay. It depends on $E_\mu^{surface} \cos \theta$ and rises from $\eta = 5.4\%$ at low energies to $\eta \times \epsilon_K / \epsilon_{pi} = 40\%$ at high $E_\mu^{surface} \cos \theta$. This substantial rise which occurs mostly between 115 GeV and 850 GeV is caused by the different masses and lifetimes of pions and kaons, not by any increased amount of kaon production from primary cosmic ray interactions in the atmosphere.

MINOS has provided the first high statistics measurements of the muon charge ratio at $E_\mu^{surface} \cos \theta > 115$ GeV. We will show that this gives the needed sensitivity for extracting information about cosmic ray produced pions and kaons separately. We also note that a similar calculation for neutrinos shows that kaons are the dominant parent for TeV neutrinos, which are the largest backgrounds for astrophysical source searches at neutrino telescopes.

The organization of this paper is as follows: In the following section, we review several measurements of the atmospheric muon charge ratio. In Section 3, we discuss some of the issues involved in measuring the charge ratio in a magnetic detector underground. In Section 4, we address particular issues related to the muon energy loss and how the muon energy at an underground detector is related to the energy in the atmosphere. In Section 5, we use Equation 2, which was based on ideas developed by Zatsepin[5], to parameterize the charge ratio in a simplified model. Zatsepin's work is the earliest reference that we have found which defines the roles of the critical energies $\epsilon_\pi = 115$ GeV and $\epsilon_K = 850$ GeV. There are two important implications from this model. First, the charge ratio depends not simply on the muon energy $E_\mu^{surface}$, but on the combination of the energy and zenith angle $E_\mu^{surface} \cos \theta$. Second, together with previous measurements at low $E_\mu^{surface} \cos \theta$, observation of the rise in the charge ratio, which mainly occurs between ϵ_π and ϵ_K , can be used to fit the meson production charge ratios K^+/K^- and π^+/π^- . In subsequent sections we discuss how this model compares to several full Monte Carlo calculations of the muon charge ratio, and how a possible difference in the spectral index of the primary cosmic Hydrogen and Helium flux might affect the interpretations.

2. Compilation of Measurements of the Atmospheric Muon Charge Ratio

Numerous measurements of the atmospheric muon charge ratio data have been made at the earth's surface, from MeV to multi-TeV energies. The Hebbeker and Timmermans 2002 compilation article [6] provides many references to these data. Figure 1 displays muon ratio data as a function of the surface energy; data from six experiments in the energy range 0.10 TeV to 10 TeV are shown.

Baxendale et al. [8] published extensive muon flux data in the momentum range 7-500 GeV/c using the Durham spectrometer. This detector consisted of magnetized iron blocks, flash tubes, and scintillation counters. The magnetic field in the three magnetized blocks was reversed regularly to reduce bias effects. Their highest energy charge ratio data point is at 358 GeV/c. The publication did not give the ratio as a function of zenith angle, and thus only the energy dependency of the charge ratio is used here.

The CosmoALEPH experiment [7] at the LEP facility at CERN published 8 data points in the 80-1600 GeV surface energy range. The cosmic ray portion of the experiment used only the hadron calorimeter and the time projection chambers. The detector was located at a depth of 320 m.w.e. Apparently the magnetic field was not reversed during data collection. The zenith range of 0-10 deg was studied, but the publication did not give the ratio as a function of zenith angle. Thus only the energy dependency of the charge ratio is used here.

The L3+C experiment [9] has published extensive muon charge ratio data at many zenith angles at momentum up to 380 GeV/c. The high accuracy and extensive angular range of this data is ideal for comparison with our parameterization of the muon charge ratio. We have used this data extensively in Section 4 of this paper.

Matsuno et al. [10] published data in the momentum range from 70 GeV/c to 20 TeV/c using the MUTRON magnetic cosmic ray spectrometer. It consists of a solid iron magnetic spectrometer, a calorimeter of 16 proportional chambers, and 48 spark chambers. Data was collected with both forward and reversed magnetic fields. The data was collected only at large zenith angles 86-89 degrees. While the data sample is large, there are only a few hundred events above 2 TeV/c.

MINOS has published data [1, 2] from both their Far Detector at Soudan, Minnesota and their Near Detector at Fermilab. Data from both detectors

was collected with both forward and reversed magnetic fields. Data is available as a function of the zenith angle.

Rastin [11] published data in the muon surface energy range from 6 - 1288 GeV using the Nottingham solid iron magnetic spectrometer. Data was collected with both forward and reversed magnetic fields.

Experiments with data points with relatively large error bars have not been included in this analysis since they are not useful for the precise studies in this paper. Experiments with charge ratio data values at energies above 100 GeV, with all data points having quoted errors greater than ± 0.1 , have not been included in our analysis; thus Hayman and Wolfendale [12], Appleton et al.[13], Nandi et al.[14], and Kremer et al. [15] are not included. Specifically, Burnett et al. [16] was not included in our study due to the absence of any published estimates of systematic error on their ratio values.

As seen in Figure 1, the ratio has an energy dependency; it is near 1.25 near 100 GeV and rises to a value near 1.4 at several TeV. The rise in the ratio has been attributed to an increasing contribution from kaon decay[3]. The data in Figure 1 could be parameterized with a linear function of $E_{\mu}^{surface}$ or a $\log(E_{\mu}^{surface})$ function, but there is no physics reason to expect a linear dependency with E, or even a $\log(E)$ dependency. We have chosen to use a different parameterization that encompasses more of the kinematics and the physics of the muon production processes, as will be described in Section 5.

3. Issues in Measuring the Charge Ratio

In this section, we review the method used for determining the muon charge, and consider some of the systematic errors which affect such a measurement. We describe the concept of Maximum Detectable Momentum, and consider two distinct types of systematic errors: bias and randomization.

Most measurements of the atmospheric muon charge ratio involve the use of a magnet to deflect the trajectory of a charged particle. The resulting curvature is used to measure both the charge sign and momentum of the muon. Depending on the size, granularity, and strength of the magnetic field, every detector has a Maximum Detectable Momentum (MDM). We define the MDM as that momentum for which a nearly straight real track will have a measured curvature (determined from a fit to points along the track) which is one standard deviation from zero. For a uniform magnetic field, the MDM is simply the reciprocal of the error (s.d.) of the curvature measurement, when the curvature is expressed in $(\text{GeV}/c)^{-1}$.

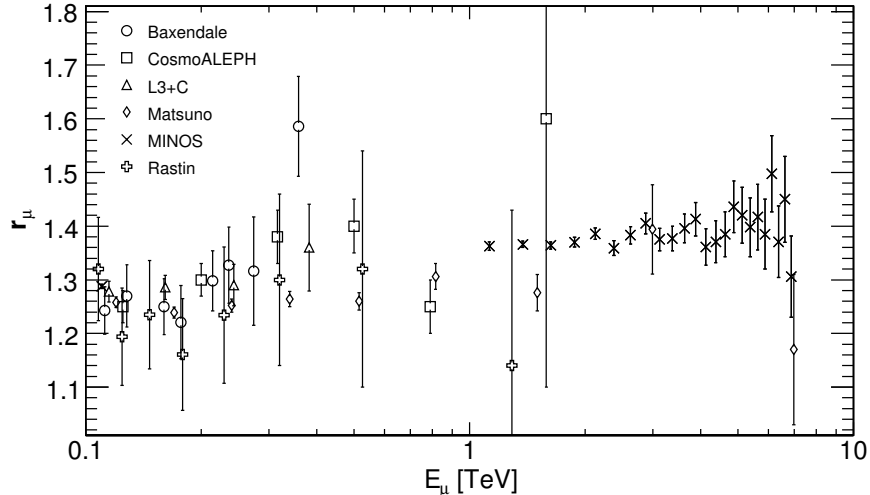


Figure 1: Compilation of muon charge ratio from experiments with at least one data point with an uncertainty less than 0.10.

The MDM can be calculated for each event in a detector. As a simplified but instructive example, we consider a simplified toroid detector which is a long right circular cylinder of radius R , with uniform density, with a B field that is azimuthal and constant. The long z -axis is perpendicular to the zenith direction. We do not consider any tracks which enter the front or leave the rear of the cylinder, i.e. all muons enter and exit the side. All such μ tracks will be roughly S shaped, with curvature one way for the first half of the track, and the other way for the second half. The length of the corresponding half-track is

$$L = \sqrt{R^2 - b^2} / \sin(\psi) \quad (3)$$

where b is the impact parameter or distance of closest approach to the center of the toroid, and ψ is the angle of the track with the z axis (not the zenith angle). For this discussion, ψ is near 90 degrees. To calculate the precision of the momentum measurement, we need the component of the magnetic field B which is perpendicular to the track direction. Approximating at the midpoint of the half-track, assuming that ψ is not small, we find

$$B_{PERP} = B \times \sqrt{[1 - \sin^2(\psi) \times \cos^2(\arctan(\sqrt{(R^2 - b^2)}/2b))]} \quad (4)$$

Equation 4 is used in Reference [10], and in Reference [17] to calculate the MDM for MINOS, which varies dramatically between 470 GeV to as low as 15 GeV for large impact parameters and large ψ , where many muon tracks occur.

The above discussion deals with the ability to measure charge in an ideal detector. In a real detector, there are a number of reasons that we might assign an incorrect charge sign to a track. We separate these errors into two kinds which we call bias and randomization. One kind of error involves biases towards one sign or the other. Other errors will cause tracks to be randomly assigned as positive or negative. These randomized events will have an apparent charge ratio of unity. Since the true charge ratio is greater than one, any such errors will lower the measured charge ratio. We next describe two instances of each kind of error.

The first kind of bias is associated with the magnetic geometry of the detector, which we call acceptance effects. Ignoring the very small magnetic field in the air outside the detector, the charge ratio of tracks which enter the detector is not affected by the magnetic field and/or the geometry of the detector. Instead, there are effects which have to do with cuts that are made to require a good track, and the efficiency of those cuts. From a given direction, tracks of one kind (the other) will be bent such that the track length in the detector is longer (shorter). In order to require a minimum number of hits to make a good charge determination, a minimum length cut may be made. Thus tracks in some directions may be biased towards one sign or the other. In the MINOS geometry, such directions occur as peaks or dips in the azimuthal distributions of the charge ratio. They tend to be symmetric with respect to the detector, but since a varying overburden can cause more tracks from some directions than others, they do not necessarily cancel.

A second kind of bias comes from any misalignment of detector planes which causes a curvature in the coordinate system. A result of any such misalignment would be that straight tracks appear to have curvature. With the MINOS geometry, it was found that a systematic misalignment of even a fraction of a mm (as measured by the track's sagitta) would have a noticeable effect on the charge ratio. A curvature cut does not remove such a bias.

Bias effects as described above are correctable in principle, with an accurate Monte Carlo. Acceptance issues can be corrected if the model of the magnetic field is accurate, and if the overburden is correctly modeled so that the expected fluxes as a function of zenith and azimuthal angle are known.

Misalignments can be modeled in principle, but must be done with a correct three-dimensional model of the detector, with an accuracy that is extremely difficult to achieve in practice.

An easier way to deal with the above bias effects is to reverse the magnetic field. If the reversal of the field is done with sufficient accuracy, then all forms of bias described above cancel when one uses the geometric mean of the charge ratio for forward and reversed field running [10]

$$r = [r_{forward} \times r_{reversed}]^{1/2} \quad (5)$$

This cancellation is apparent when one considers the ratio of the positive muons in forward(reverse) running to negative muons in reverse(forward) running. The equality of these two values is a powerful consistency check.

By contrast, effects which tend to randomize the charge ratio do not typically cancel in this manner and must be dealt with separately. An obvious type of randomization occurs for high momentum straight tracks above the MDM. If a track is straight within the resolution of the detector, then we will be unable to accurately determine the charge sign. For a straight enough track, a program will measure curvature either way an equal fraction of the time. The fit that calculates the curvature can also calculate the error on the curvature. This form of randomization can be minimized by cutting on the fractional curvature error $\sigma(1/p)/(1/p)$ as is shown in Figure 5 of Reference [1]. However the fraction of mismeasured tracks may not follow a Gaussian distribution for $\sigma(1/p)/(1/p)$ and Monte Carlo estimates of the misidentification must be analyzed with care.

A second form of randomization, which was observed in MINOS data, was generally associated with extra hits. These might be due to noise, crosstalk or demultiplexing issues, or also delta rays or other particles associated with the muon. For beam experiments, the magnetic field is perpendicular to the beam direction, to maximize bending power from the magnet. For cosmic rays, muons are observed at all angles. As described above, muon tracks will be bent much more in a toroidal magnet if they impinge on the detector with a low impact parameter. For those cosmic ray muons which are traveling mostly parallel to the magnetic field (at large impact parameter), an interesting situation can arise if the apparent bending due to multiple scattering is comparable to the bending from the magnetic field. If that happens, a reconstruction program which takes into account multiple scattering can get a good fit for a straight track for any momentum. The inclusion of a hit or

hits which do not belong on the track can then lead to a class of muon tracks which are really at high momentum, but get reconstructed at low momentum with a random charge sign depending on which side of the track the extra hits appeared.

We can quantify this result as follows: Projected onto a plane, the RMS multiple Coulomb scattering angle can be written

$$\langle \theta_{MCS} \rangle = [0.0136/p(\text{GeV}/c)] * \sqrt{(L(\text{meter})/X)} \quad (6)$$

where X is the radiation length. The magnetic bending for this same length of track is given by

$$\theta_{Bend} = L(\text{meter}) * B_{PERP}(\text{Tesla})/[3.336 * p(\text{GeV}/c)] \quad (7)$$

Note that in the ratio $\theta_{MCS}/\theta_{Bend}$, p cancels. For typical muon tracks in MINOS, the ratio rises from 0.14 at low impact parameter and ψ to near unity at large impact parameter. Thus the type of randomization described in the previous paragraph can be preferentially removed by discarding events with large values of $\langle \theta_{MCS} \rangle / \theta_{Bend}$.

The cancellation of bias effects can be checked by studying distributions which have bias effects in them before and after the forward and reverse field data are combined. We have no such consistency check for randomization effects. Thus, the ability to detect and control all bias effects using the combined forward and reverse field data is stronger than the ability to cancel all randomization effects. This might lead to a tendency for experiments to report a charge ratio which is systematically smaller than the true value. We also note that not every experiment listed in Section 2 has taken data with a reversed magnetic field.

4. Issues with Interpreting Data Obtained Underground

4.1. The Relevance of Energy Loss Differences

The charge ratio measured in underground experiments is a ratio of μ^+ to μ^- at the detector. For comparison with production models, the relevant quantity is the ratio in the upper atmosphere. If the energy loss of positive and negative muons were identical, as they go through the earth, these two ratios would be the same. The leading energy loss processes of μ^+ and μ^- are the same of course, but there are corrections of the order of the fine structure constant α . We evaluate these small differences, first for ionization

energy loss, and then for radiative processes. The latter difference is found to be negligible. The small difference in ionization energy loss is used to calculate the difference in range and the correction to the charge asymmetry as a function of slant depth in Section 4.4.

The statistical energy loss of muons, traversing an amount X of matter in g/cm^2 , with energies far above the Bethe-Bloch minimum is usually parameterized as

$$-\frac{dE_\mu}{dX} = a(E_\mu) + \sum_{n=1}^3 b_n(E_\mu) \cdot E_\mu, \quad (8)$$

where a is the collisional term (i.e. ionization) and b in the second term accounts for the three radiative muon energy loss processes: Bremsstrahlung, pair production and photo-nuclear interactions. In Table 1[18][19] these energy loss parameters are listed for standard rock. The critical energy where ionization losses equal radiative losses in standard rock is approximately 0.6 TeV. The average muon surface energy for a muon which reaches 2000 mwe is greater than 1 TeV, so the b term and its energy dependence are important in calculating the energy loss. We have investigated differences in the a and b terms for μ^+ and μ^- .

E_μ [GeV]	a_{ion} [MeV cm ² /g]	b_{brems}	b_{pair}	b_{DIS}	Σb
		10 ⁻⁶ cm ² /g			
10	2.17	0.70	0.70	0.50	1.90
10 ²	2.44	1.10	1.53	0.41	3.04
10 ³	2.68	1.44	2.07	0.41	3.92
10 ⁴	2.93	1.62	2.27	0.46	4.35

Table 1: Average muon energy loss parameters calculated for standard rock [18][19]

4.2. Difference in Ionization dE/dx for μ^+ and μ^-

At low energies, around the Bethe-Bloch minimum, the difference in ionization energy loss is known as the Barkas effect[20], and there have been efforts to both measure and calculate the difference[21]. Calculations show that negative particles lose energy at a slower rate, with the difference dropping from tens of percent at MeV energies to about 0.3% in the GeV range.

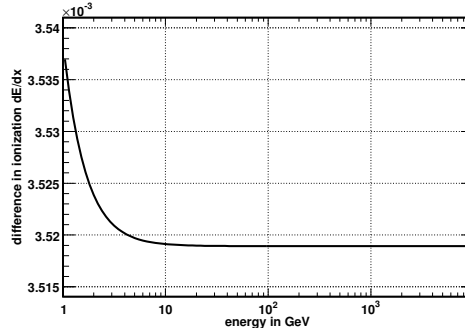


Figure 2: Calculated difference in ionization energy loss between positive and negative muons in standard rock (average nuclear properties: $\bar{Z} = 11$, $\bar{A} = 22$ [19]).

Such differences were experimentally verified both at MeV energies[22][23][24] and in the GeV range [25]. At higher energies, this difference in ionization energy loss has usually been neglected, and we are not aware of any measurements. As described in Reference [26], the usual ionization energy loss term for muons (of either sign) depends on z^2 , and the difference between μ^+ and μ^- arises from a small additional z^3 correction term. This correction term in dE/dx is:

$$\left(\frac{dE}{dX}\right)_{ion}^{corr} = \frac{\pi\alpha z^3 0.307Z}{2\beta A} \quad [MeV cm^2 g^{-1}] \quad (9)$$

where α is the fine structure constant, z is the charge, β is the relativistic velocity, and Z and A are the nuclear properties of the material through which the muon is passing. The absolute value of the difference in ionization energy loss between positive and negative muons in standard rock[19] is plotted in Figure 2. It is fairly constant above 10 GeV, at a value corresponding to approximately 0.15% of the mean energy loss in the ionization dominated energy regime (*c.f.* Table 1)[27].

4.3. Calculated Difference in Bremsstrahlung dE/dX for μ^+ and μ^-

Above an energy near 0.6 TeV in standard rock, radiative energy loss becomes comparable to ionization energy loss, and continues to grow at higher muon energies. Radiative energy loss has been calculated using the Eikonal approximation in References [28] and [29]. For the difference between positive

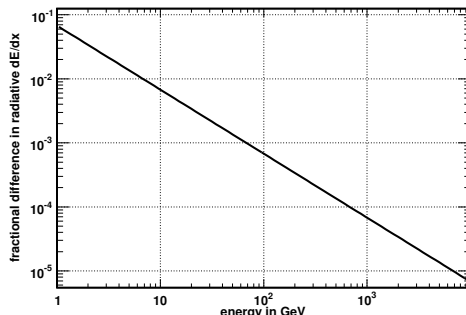


Figure 3: Calculated fractional difference in Bremsstrahlung energy loss between positive and negative muons.

and negative particles, the leading term cancels, and only a term proportional to $M/E = 1/\gamma$ survives, which does depend on the sign of the charge[30]:

$$\frac{[\frac{dE}{dX}]_{brems}^{\mu^+} - [\frac{dE}{dX}]_{brems}^{\mu^-}}{[\frac{dE}{dX}]_{brems}} = \frac{8Z\alpha}{\gamma} \quad (10)$$

where γ is the Lorentz factor of the muon. Again, the μ^+ has a slightly higher energy loss. This fractional difference *decreases* with energy and is already negligible where radiative energy losses become important. This fractional difference is plotted in Figure 3 for muons in standard rock. Presumably, the same fractional difference can also be assigned for pair-production, as the underlying process is a two-photon exchange between the muon and the constituents of the nucleus, and thus the cross sections for μ^+ and μ^- should scale in the same way as for Bremsstrahlung.

4.4. Range Underground and Muon Charge Asymmetry

Taking the vertical muon intensity from the Gaisser parameterization of the muon flux at the surface (see Equation 2) and propagating this energy spectrum underground according to statistical ionization and radiative energy losses, one can calculate the underground muon intensity. This procedure is described in detail in [31] for overburdens of standard and Soudan rock (MINOS). First, the average muon range underground, for each value of surface energy, is computed. For this, the energy dependent a and Σb values were parameterized for standard and Soudan rock as in [31]. The additional

ionization loss according to Equation 9 was added for μ^+ to the value of the function for a (subtracted for μ^-). Radiative losses (90% of Σb) were scaled with the energy dependent fractional difference $8Z\alpha/\gamma$ according to Equation 10 as $\Sigma b^\pm = 0.9 \cdot \Sigma b \cdot (1 \pm 4Z\alpha/\gamma)$ for μ^+ and μ^- , respectively. The contribution from photo-nuclear production (DIS), was not scaled. For each initial value of muon energy, the slant depth in meter-water-equivalent where the muons of different charge range out was determined.

We computed the underground intensities of positive and negative muons as a function of slant depth for a given rock composition. This ratio of the μ^+ and μ^- intensity curves is shown in Figure 4 for Soudan rock. The upper curve corresponds to the fractional difference in integral intensities of μ^+ and μ^- at a given slant depth. For slant depth values above about 1000 mwe the underground ratio $N(\mu^+)/N(\mu^-)$ is lowered by roughly 0.4%. The detected intensity corresponds to the charge ratio of the muons at depth below the MDM for MINOS. For increasing slant depth values the measured underground ratio $N(\mu^+)/N(\mu^-)$ is further reduced and saturates at about 0.6% below its surface value for slant depths larger than roughly 5000 mwe.

The small fractional difference in energy loss for μ^+ and μ^- of the order of 0.15% predicted by theoretical calculations at high energies, gets amplified by a factor of about 3.7, due to the approximate $E^{-3.7}$ dependence of the differential muon spectrum. The impact of the rock composition is almost negligible, as the induced muon charge asymmetry under Soudan rock lowers the surface value of the ratio by an additional amount less than 0.02% compared to standard rock. Figure 4 can be used to correct the underground measured muon charge ratio to its surface value. For MINOS, this corresponds to a correction which increases the measured value by 0.6%.

5. Model of Pion and Kaon Contributions to the Charge Ratio

We have investigated a generalization of Gaisser's Equation 2 to study separately the positive and negative muon intensities. Using the positive fraction parameters f_π and f_K , the energy dependency of the positive and negative muons is given by

$$\frac{dN_{\mu^\pm}}{dE_\mu} = \frac{0.14E_\mu^{-2.7}}{\text{cm}^2 \text{ s sr GeV}} \times \left\{ \frac{f_\pi}{1 + \frac{1.1E_\mu \cos \theta}{115 \text{ GeV}}} + \frac{\eta \times f_K}{1 + \frac{1.1E_\mu \cos \theta}{850 \text{ GeV}}} \right\} \quad (11)$$

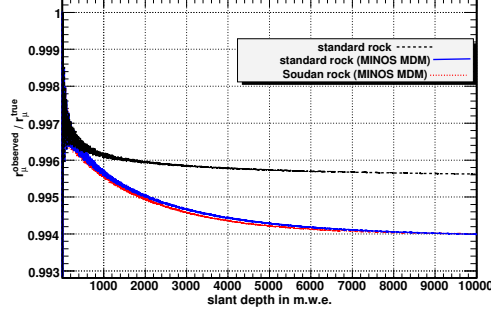


Figure 4: Calculated ratio of positive to negative vertical muon intensities in Soudan rock as a function of slant depth for equal surface intensities. The upper curve is for all muons, the lower curve is for muons with a remnant momentum of less than 250 GeV/c (\approx the maximum detectable momentum in the MINOS Far Detector).

$$\frac{dN_{\mu^-}}{dE_{\mu}} = \frac{0.14E_{\mu}^{-2.7}}{\text{cm}^2 \text{ s sr GeV}} \times \left\{ \frac{1 - f_{\pi}}{1 + \frac{1.1E_{\mu} \cos \theta}{115 \text{ GeV}}} + \frac{\eta \times (1 - f_K)}{1 + \frac{1.1E_{\mu} \cos \theta}{850 \text{ GeV}}} \right\} \quad (12)$$

where ϵ_{π} and ϵ_K have been replaced by their numerical values. We can use equations 11 and 12 to calculate the surface muon charge ratio:

$$r_{\mu} = \frac{\left\{ \frac{f_{\pi}}{1 + 1.1E_{\mu} \cos \theta / 115 \text{ GeV}} + \frac{\eta \times f_K}{1 + 1.1E_{\mu} \cos \theta / 850 \text{ GeV}} \right\}}{\left\{ \frac{1 - f_{\pi}}{1 + 1.1E_{\mu} \cos \theta / 115 \text{ GeV}} + \frac{\eta \times (1 - f_K)}{1 + 1.1E_{\mu} \cos \theta / 850 \text{ GeV}} \right\}} \quad (13)$$

The charge ratio of muons from pion decay is $r_{\pi} = f_{\pi}/(1 - f_{\pi})$ and from kaon decay is $r_K = f_K/(1 - f_K)$. We will refer to the implications of Equation 13 with energy independent parameters as the “pika” model. There are several interesting features of this model:

1. The relative intensity of cosmic ray pions and kaons that contribute to muon production can be extracted from surface and underground muon charge ratio experiments.
2. The muon charge ratio does not depend upon the muon energy and the zenith angle separately, but on the product $E_{\mu}^{surface} \cos \theta$. This product of terms controls the relative portions of interaction and decay for both pions and kaons. At a fixed value of $E_{\mu}^{surface} \cos \theta$, the intensity ratio of muons from pions and kaons is constant.

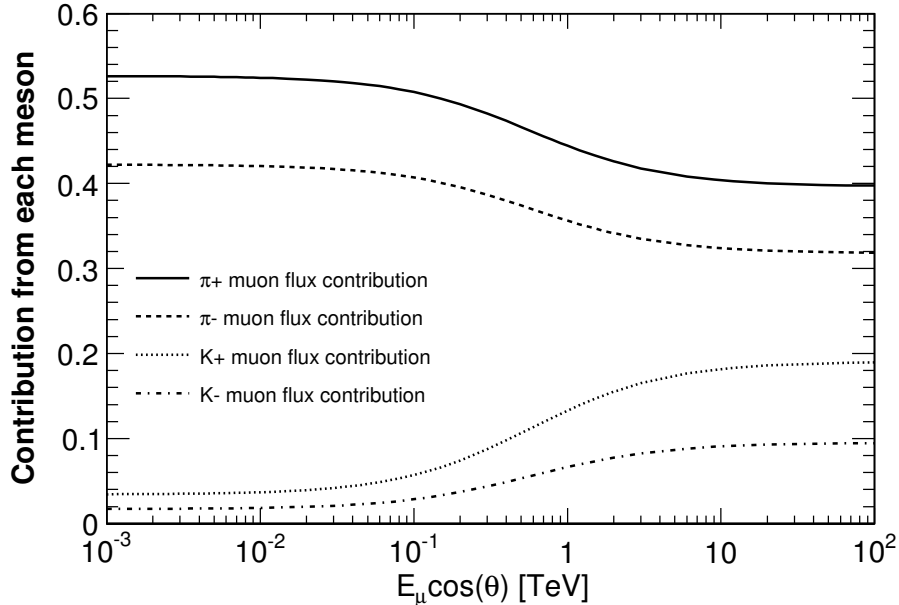


Figure 5: Contributions to the muon flux from the four mesons using the pika model

3. There are contributions to the muon charge ratio r_μ from both pions and kaons from 1 GeV to 10 TeV. The contribution to the ratio from kaons does not vanish at GeV energies - it is just smaller than at TeV energies. This effect can be seen in Figure 5 which displays the contribution to the muon flux from each of the four mesons.
4. The pika model postulates an energy independent $r_\pi = \pi^+/\pi^-$ ratio related to f_π , and energy independent $r_K = K^+/K^-$ ratio related to f_K , and an energy independent π/K ratio embodied in the Gaisser constant 0.054.
5. Contributions from charm particle production have been ignored because their effect on the ratio below 10 TeV is expected to be negligible.

Where Feynman scaling is valid, the fraction $x = E_{meson}/E_{proton}$ for π and K secondaries does not depend upon E_{proton} . Then f_π and f_K are also energy independent. Here we explore features of our simple model, and in the next section we shall compare the qualitative features of our model with full simulations of the charge ratio.

Our parameterization yields additional insight into the sensitivity of var-

ious underground experiments which measure the muon charge ratio. Underground experiments can effectively observe a much smaller range of $E_\mu^{surface} \cos \theta$ than a range of E . To see this, consider a simple approximation with five assumptions:

1. The parameter a in Equation 8 is constant
2. The parameter b in Equation 8 is constant and set to zero.
3. The earth/rock density above the underground detector is constant
4. The surface above the detector is flat
5. The MDM in the underground detector is negligible compared to the energy loss from the surface to the detector.

The first four assumptions are equivalent to stating that the muon energy loss in the earth is proportional to the overburden which only depends upon the muon zenith angle. In that case the energy loss through the overburden is $E_{loss} = E_{min}/\cos(\theta)$, where E_{min} is the minimum energy loss for a vertical cosmic muon. The fifth assumption implies that the underground energy of the muons used for the charge ratio measurement is much smaller than their surface momentum.

With these five assumptions, the muon intensity distribution in $E_\mu^{surface} \cos \theta$ would be measured to be a delta function at a value of E_{min} . While at large zenith angles the surface energy increases due to the $1/\cos(\theta)$ dependence of the slant depth, the combined quantity $E_\mu^{surface} \cos \theta$ remains constant. It is illuminating to compare this naive prediction to the actual distribution in the MINOS detectors when no such assumptions are made. These are shown in Figures 6 and 7. Both of these MINOS $E_\mu^{surface} \cos \theta$ distributions are considerably narrower than the corresponding $E_{surface}$ distributions. The $b(E)$ radiative term yields the largest contribution to the width of the measured $E_\mu^{surface} \cos \theta$ distribution for the MINOS Far Detector. In the Near Detector distribution, the largest contribution is the larger ratio of maximum detectable momentum to energy loss in the overburden.

We have used Equation 13 and the measured muon charge ratio to study r_π and r_K . We have done chi-squared fits in $E_\mu^{surface} \cos \theta$ to the MINOS Near Detector and Far Detector data, and to the L3+C data. The fit yields $f_\pi = 0.5510 \pm 0.0006$ and $f_K = 0.7006 \pm 0.0061$. These values lead to a muon charge ratio from pion decay of $r_\pi = 1.227 \pm 0.003$ and a muon charge ratio from charged kaon decay of $r_K = 2.34 \pm 0.07$. The errors in the two parameters are highly correlated. This fit is shown in Figure 8 along with

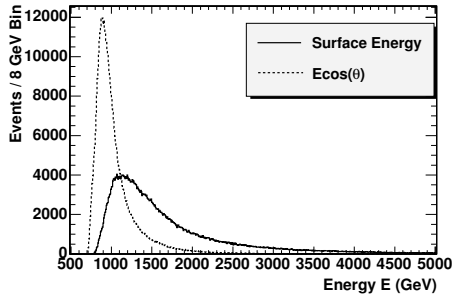


Figure 6: Distribution of E and $E_{\mu}^{surface} \cos \theta$ for MINOS data muons in the Far Detector, after cuts (GeV).

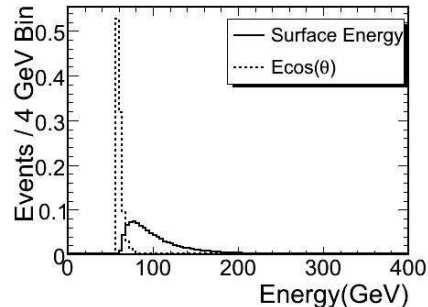


Figure 7: Distribution of E and $E_{\mu}^{surface} \cos \theta$ for MINOS data muons in the Near Detector, after cuts (GeV).

the MINOS (Near and Far) and L3+C data. The agreement between the parametrization and the data is excellent.

Using the f values from this fit, we plot Equation 13 for an extended range of muon energy in Figure 9. The critical energies discussed above for pion and kaons are indicated by the arrows. The low energy asymptotic ratio is $(f_{\pi} + \eta f_K) / [1 - f_{\pi} + \eta(1 - f_K)] = 1.26$. The high energy ratio is $(\epsilon_{\pi} f_{\pi} + \epsilon_K \eta f_K) / [\epsilon_{\pi}(1 - f_{\pi}) + \epsilon_K \eta(1 - f_K)] = 1.45$. The low and high energy asymptotic values both include muons from π decay and from K decay.

The fit was repeated using just the smaller data sample of the MINOS Near Detector[32] and Far Detector. We obtain $f_{\pi} = 0.5483 \pm 0.0011$ and $f_K = 0.7117 \pm 0.0074$, which imply $r_{\pi} = 1.219 \pm 0.004$ and $r_K = 2.47 \pm 0.08$.

The parameterization we have used seems sufficient to represent the published data sets.

Our fits to r_{π} gives values near expectations. Our fit to $r_K = K^+/K^-$ in atmospheric showers yield values near 2.3. It is clearly difficult to directly measure the atmospheric kaon charge ratio. Equation 13 provides a well defined parametrization for future studies of this subject.

6. Comparison with Full Simulations of Atmospheric Muons

Full simulations of the muon charge ratio have been published by Honda [34], CORT [3], and Lipari[33]. These model results of the ratio versus the muon surface energy $E_{\mu}^{surface}$ are displayed in Figures 10, 11, and 12 for various ranges of $\cos(\theta)$. The Honda results show small dependencies upon

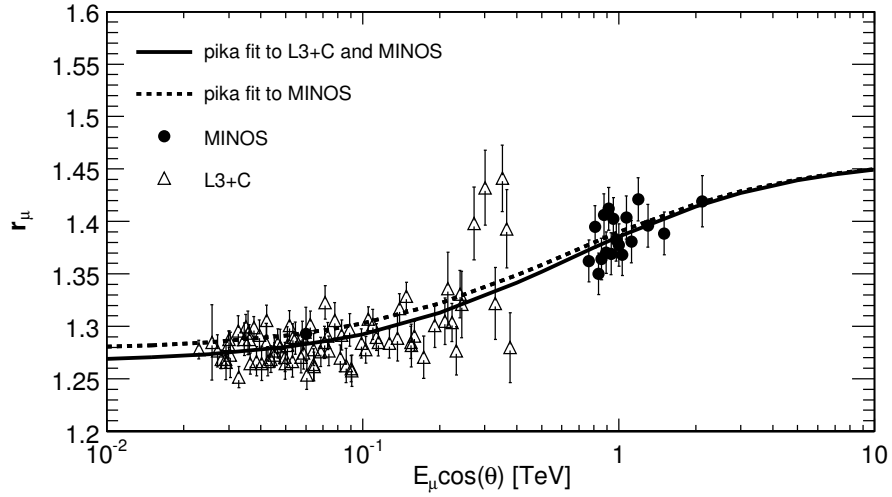


Figure 8: Pika model fitted to L3+C and MINOS (Near and Far) data sets

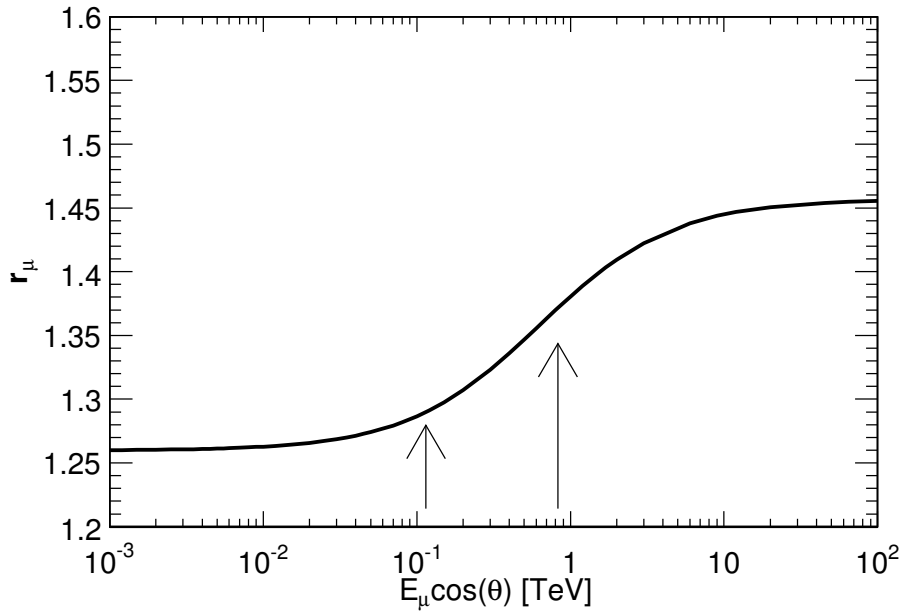


Figure 9: The pika model's muon charge ratio for an extended range of energy. The critical energies for pion and kaon decay vs interaction are shown by the arrows.

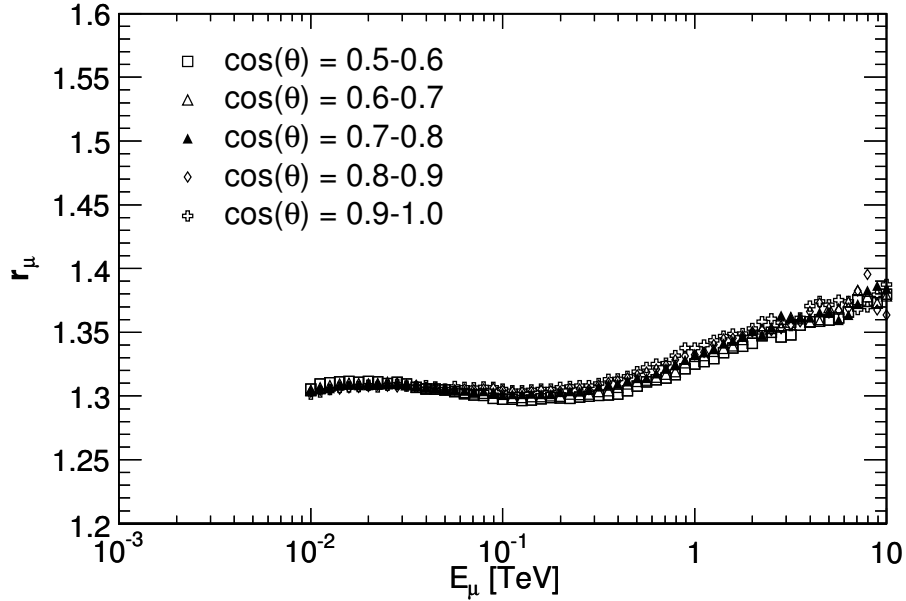


Figure 10: Honda calculations of the muon charge ratio at 5 zenith angles

the zenith angle, and an interesting dip in the ratio near 200 GeV. The CORT results show a larger dependency upon the zenith angle as the energy increases. The Lipari results show even a larger dependency upon zenith angle at energies above 10 GeV. The results from the models differ noticeably from each other and from the MINOS and L3+C data sets. None of the authors of these models discuss the dependency of their results on the variable $E_\mu^{surface} \cos \theta$.

In our analysis, we do investigate (1) the dependency of these charge ratio simulations on the $E_\mu^{surface} \cos \theta$ variable discussed in the previous section of this paper, and (2) their consistency with the pika model of the charge ratio. Our observation will be that $E_\mu^{surface} \cos \theta$ is a more useful variable for ratio analysis than just the muon energy $E_\mu^{surface}$.

Figure 13 displays Honda's muon charge ratio simulations as a function of $E_\mu^{surface} \cos \theta$ using published values from five ranges of $\cos(\theta)$ from 0.3 to 1.0. For a wide range of the variable $E_\mu^{surface} \cos \theta$, the charge ratio is nearly independent of $\cos(\theta)$, consistent with the representation of the pika model.

Figure 14 displays the corresponding CORT theory simulations of the

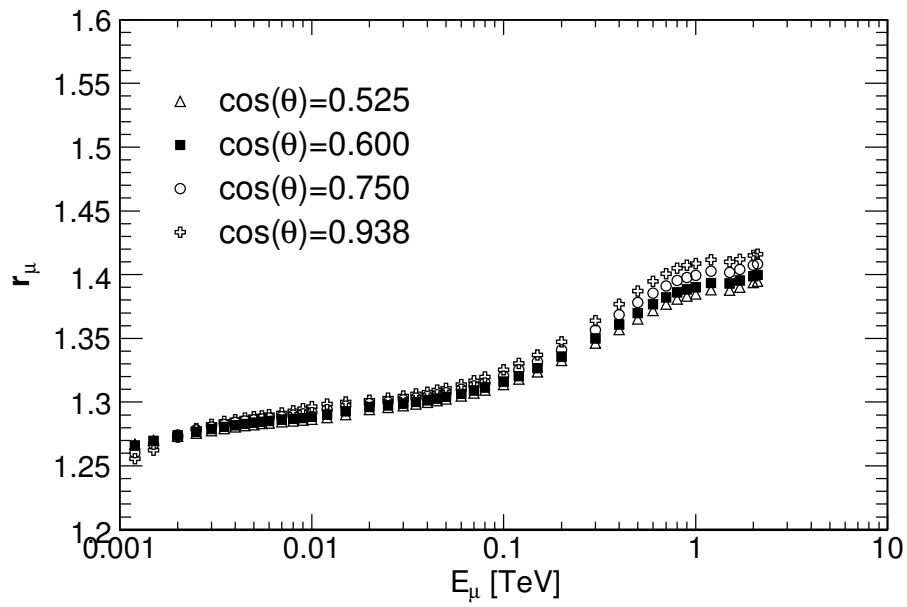


Figure 11: CORT calculations of the muon charge ratio at 4 zenith angles

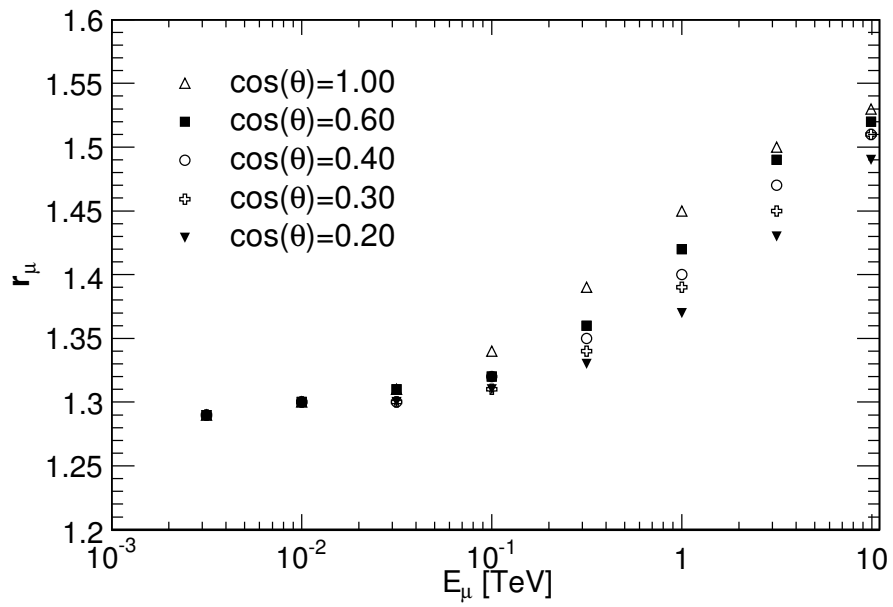


Figure 12: Lipari calculations of the muon charge ratio at 5 zenith angles

charge ratio as a function of $E_\mu^{surface} \cos \theta$ using four published values of $\cos(\theta)$. In the $E_\mu^{surface} \cos \theta$ range from 5 GeV to 600 GeV, the simulations show minimal dependency on $\cos(\theta)$. Above 600 GeV, the charge ratio model results do increase with increasing values of $\cos(\theta)$. The prediction of the pika model that the ratio is independent of $E_\mu^{surface} \cos \theta$ is consistent with the CORT simulation for a remarkable range of $E_\mu^{surface} \cos \theta$.

Figure 15 displays the Lipari simulations of the charge ratio as a function of $E_\mu^{surface} \cos \theta$ for five values of $\cos(\theta)$ from 0.2 to 1.0. It is apparent that a significant portion of the ratio variation with $\cos(\theta)$ is minimal when the ratio is displayed as a function of $E_\mu^{surface} \cos \theta$. Again, the pika model prediction of a charge ratio independent of $E_\mu^{surface} \cos \theta$ is consistent with the Lipari simulation over four orders of magnitude in $E_\mu^{surface} \cos \theta$.

The observed dependence of the above three simulations on $E_\mu^{surface} \cos \theta$ provides support for analyzing the charge ratio data using the pika formula. Of course it would be interesting to understand the source of the remaining variations in the simulations as a function of $E_\mu^{surface} \cos \theta$.

Next we quantitatively compare the pika model to the three simulations discussed above. Two parameter chi-squared fits were performed to the simulation's ratio values assuming equal uncertainties on each point within a simulation. The best fit for each simulation is shown as a smooth line in the corresponding figure. For the CORT model, the pika model fits well the simulation from 20 GeV to 600 GeV at all angles. The fit yields $f_\pi = 0.557$ and $f_K = 0.705$. For the Honda simulation, the pika model can not reproduce the simulation's dip at ~ 200 GeV, although it does describe the simulation's overall energy dependency from 5 GeV to 5 TeV. The Honda fit yields $f_\pi = 0.5615$ and $f_K = 0.6207$. For the Lipari simulation, the pika model reproduces well the simulation from 3 GeV to 10 TeV. The fit yields $f_\pi = 0.5551$ and $f_K = 0.7413$. To summarize, we conclude there is physics content in using the variable $E_\mu^{surface} \cos \theta$ in studying the results of these three simulations. However, the pika model can not reproduce the full richness of these simulations, and of course the fitted pika parameters are significantly different among the three simulations.

To complete this study, we have compared the L3+C and MINOS charge ratio data sets to the same three simulations. So as to concisely represent the three simulations, we have used the fits of the three simulations to the pika model to compare with data. As seen in Figure 16, none of the models (as parameterized by the pika formula with varying degrees of success) correctly predicts the charge ratio data's magnitude and dependency upon

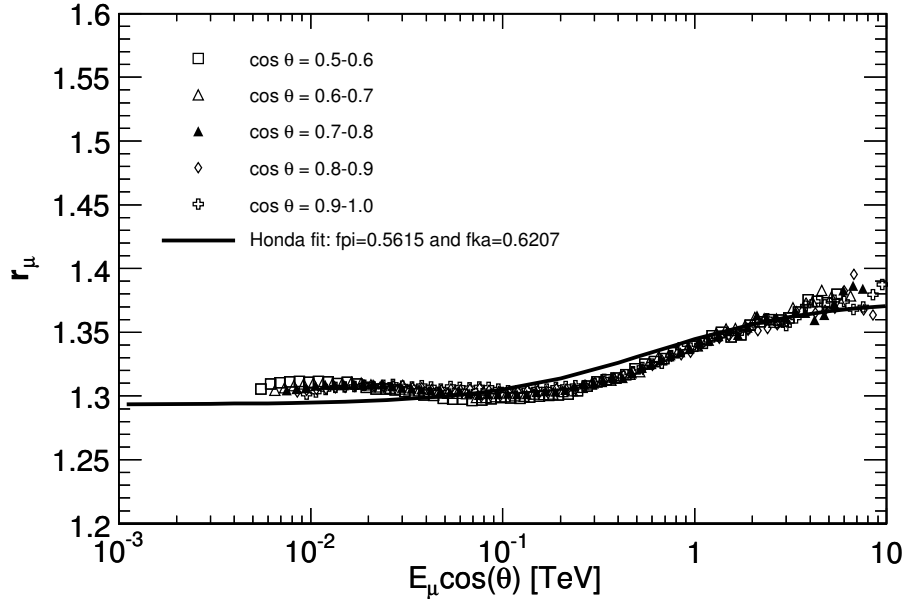


Figure 13: Honda calculations of the muon charge ratio vs $E_{\mu}^{surface} \cos \theta$ at 5 zenith angles. The curve is a fit of these simulation results to the pika model.

$E_{\mu}^{surface} \cos \theta$. Comparing the pika model results shown in Figure 9 and Figure 16, it is apparent that none of the three simulations are using optimal values of f_{π} and f_K . This can be seen in Table 3 and is discussed further in Section 8.

7. Effect of Helium on the Charge Ratio

Another process that could affect the energy dependence of r_{μ} would be a different spectral index for the heavier cosmic ray primary flux than for the proton flux. This would introduce an energy dependence to the incoming proton to neutron ratio. It is not well established that the energy dependence of the heavy primary intensities is different than that for Hydrogen in the 10 TeV energy range. For this study, we will use Gaisser and Honda's [35] parameterizations of the primary flux as a function primary component k with energy E_k , given as

$$\phi(E_k) = K(E_k + b \times \exp[-c\sqrt{(E_k)}])^{-\alpha} \quad (14)$$

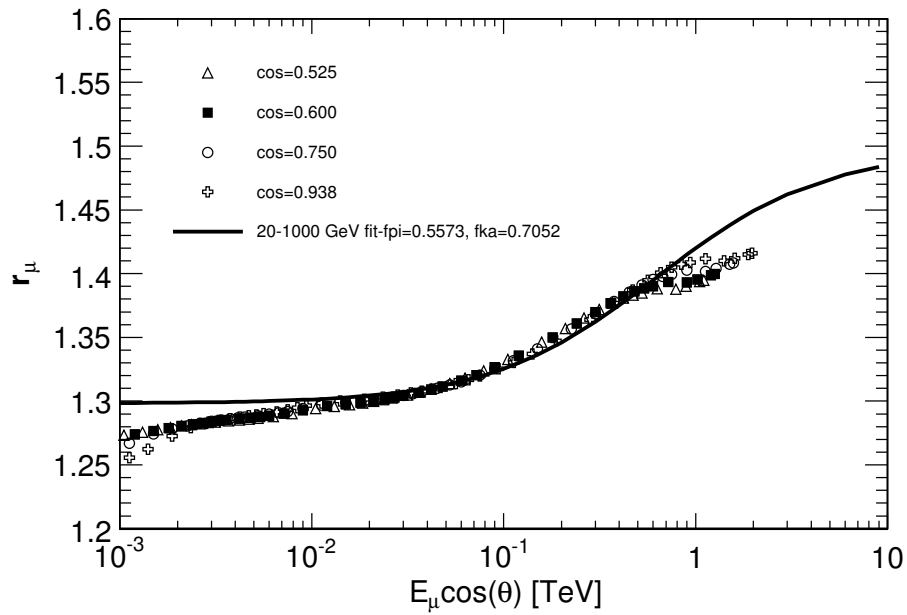


Figure 14: CORT calculations of the muon charge ratio vs $E_\mu^{surface} \cos \theta$ at 4 zenith angles. The curve is a fit of these simulation results to the pika model.

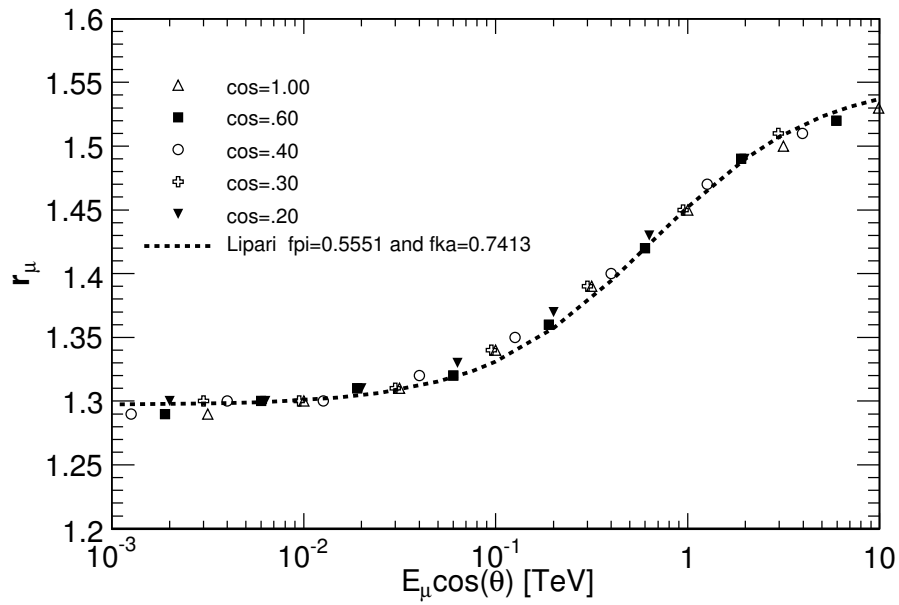


Figure 15: Lipari calculations of the muon charge ratio vs $E_\mu^{surface} \cos \theta$ at 5 zenith angles. The curve is a fit of these simulation results to the pika model.

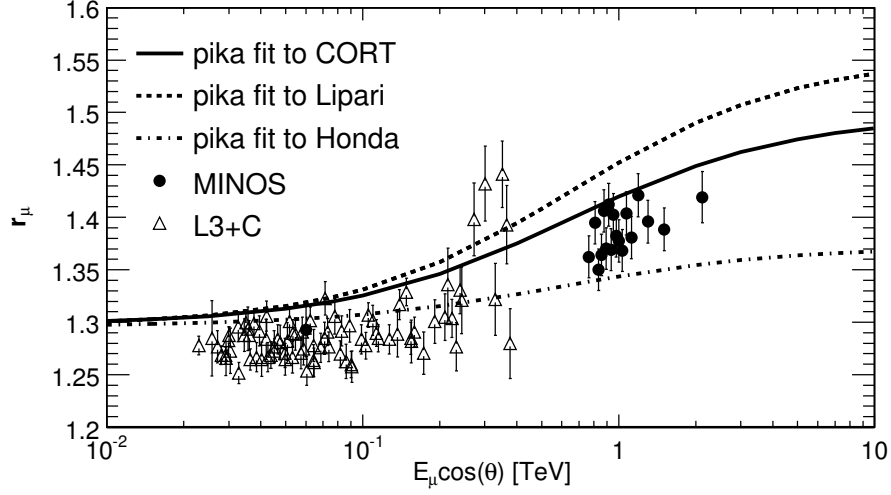


Figure 16: Fits of the pika model to the three simulation models of the charge ratio vs $E_{\mu}^{surface} \cos \theta$ compared to L3+C and MINOS data sets.

The parameters in the above equation are given in the Table 2 below. Note that this reference has a spectral index decreasing slightly with increasing primary mass.

Parameter	α	K	b	c
Hydrogen	2.74 ± 0.01	14900 ± 600	2.15	0.21
He (A=4)	2.64 ± 0.01	600 ± 30	1.25	0.14
CNO (A=14)	2.60 ± 0.07	33.2 ± 5	0.97	0.01

Table 2: Primary flux parameters used in the text.

Figure 17 displays the contributions to the flux as a function of the kinetic energy per nucleon. Based on Monte Carlo calculations using CORSIKA, the mean surface energy of muons which reach 2100 mwe underground is 9% of the primary nucleon energy. The mean fraction of the primary Helium energy, per nucleon, that is transferred to the muon is 11%. We will assume the fraction of the energy transfer for primary carbon, nitrogen, and oxygen to be identical to that of Helium. In the following calculations, the energy profiles of the protons and Helium from Monte Carlo are used instead of

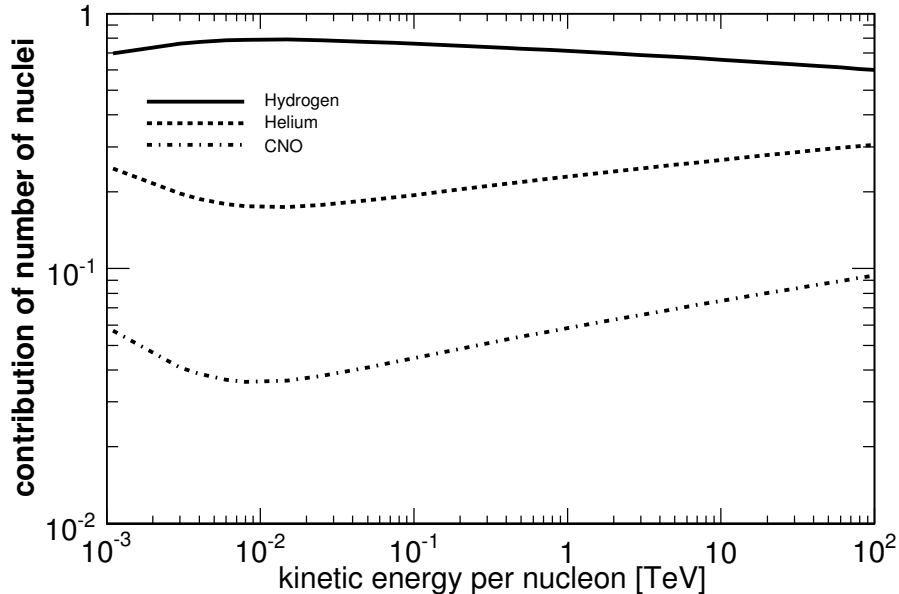


Figure 17: Fractional contribution of nuclei to the all nucleon spectrum

these average values, although the effect is not large.

We will calculate the corrections to the fitted f_π and f_K parameters in Equation 13 to account for the possible energy dependency of the incoming proton to neutron ratio (due to the Helium and CNO flux). We use a model to estimate the impact of both pion and kaon production by protons and neutrons. We assume two contributions for meson production: pair production of equal number of positive and negative mesons, and leading particle production using quark counting to estimate the excess. This calculation will use meson charge ratios near the previous fit values. We start with $r_\pi = 1.25$ and $r_K = 2.61$ and see how much they change due to the different spectral index for H and He.

First we will model the change in the muon charge ratio due to just pion decay when Helium and CNO are added to the primary proton flux. Using CORSIKA separately for cosmic ray protons and Helium of energy E_{CR} , we have calculated weights w^i in 11 bins of the ratio E_μ/E_{CR} . In a simple quark model the leading proton and neutron particle in the forward direction will give rise to a charge ratio of 1.00 for symmetric nuclei $A-Z=Z$.

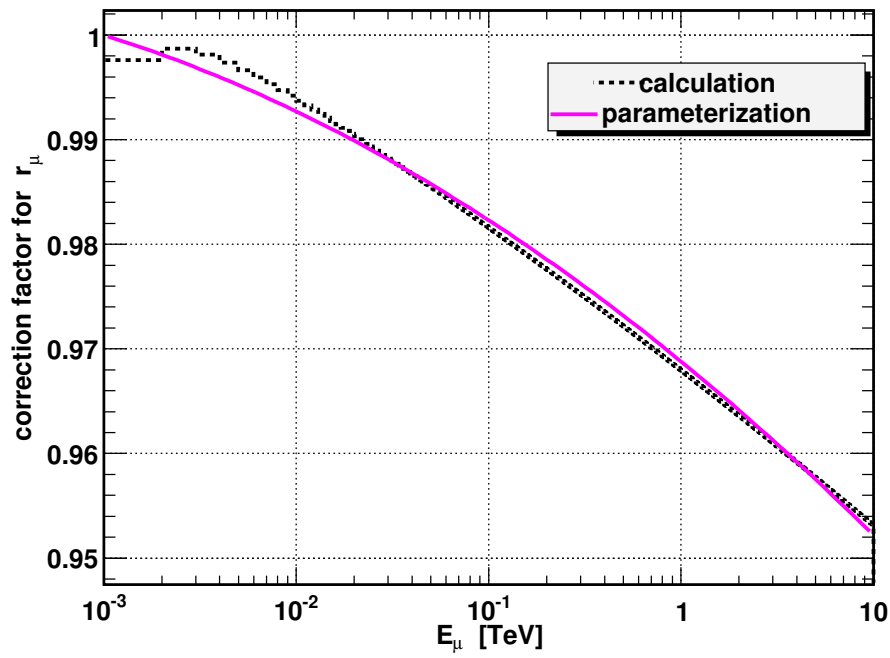


Figure 18: Correction factor for r_μ assuming a different energy spectrum for Helium from pion production only.

Setting the muon charge ratio equal to 1.25 at 1 GeV and fixing the normalization of the Hydrogen flux to be 1.317 (in order to get back the charge ratio of 1.25 at 1 GeV), one has for the muon charge ratio

$$r^\pi(E_\mu) = \frac{\sum_{i=0}^{10} [0.5 \times (w_p^i + w_{He}^i) \times w_p^i 1.317 \times \phi_p(E_{CR}) + w_{He}^i 1.0 \times 4\phi_{He}(E_{CR}) + w_{He}^i 1.0 \times 14\phi_{CNO}(E_{CR})]}{w_p^i \phi_p(E_{CR}) + w_{He}^i 4\phi_{He}(E_{CR}) + w_{He}^i 14\phi_{CNO}(E_{CR})} \quad (15)$$

The 1.0 values are due to the equal production rates of leading π^+ and π^- in our quark counting model.

A subtlety of our notation is that the π (and K) superscript represents the energy dependent correction to the charge ratio arising from the different possible spectral index of heavy cosmic ray primaries, while the subscript represents the assumed energy independent meson ratio. Figure 18 displays the corresponding fractional change in the charge ratio as a function of the muon surface energy. Note that the effect is about a 3 percent reduction at 1 TeV. This dependency can be fit to a polynomial in $\log(E)$, also shown in Figure 18, with the result

$$r^\pi(E_\mu)/1.25 = 1 - 0.00575 \times \log_{10}(E_\mu/GeV) - 0.00155 \times \log_{10}^2(E_\mu/GeV) \quad (16)$$

Next we include the contribution from kaon production by the primaries. The cross section for associated production of ΛK^+ is much larger than that for K^+K^- pairs for both incident protons and neutrons. Again assuming a quark model for the leading kaon in the forward direction from incident protons and neutrons, one only gets leading K^+ , but twice as many from protons than from neutrons corresponding to their number of u quarks.

$$p(uud) + air \rightarrow K^+(u\bar{s}) + \dots \quad (17)$$

and

$$n(ddd) + air \rightarrow K^+(u\bar{s}) + \dots \quad (18)$$

In this model, the positive kaon excess originating from protons ($r_K - 1$) is twice as large as the excess originating from neutrons. For symmetric nuclei

with $A-Z=Z$ this leads to a charge ratio

$$1 + \frac{[1 + 1/2]}{2}(r_K - 1) = 1/4 + 3r_K/4 \quad (19)$$

We further assume that the muon charge ratio at 1 TeV is 1.374 (near the MINOS value). This then yields

$$r^K(E_\mu) = \frac{\sum_{i=0}^{10} [0.5 \times (w_p^i + w_{He}^i) \times w_p^i 2.7 \times \phi_p(E_{CR}) + w_{He}^i 2.275 \times 4\phi_{He}(E_{CR}) + w_{He}^i 2.275 \times 14\phi_{CNO}(E_{CR})]}{w_p^i \phi_p(E_{CR}) + w_{He}^i 4\phi_{He}(E_{CR}) + w_{He}^i 14\phi_{CNO}(E_{CR})} \quad (20)$$

The value 2.275 is due to Equation 19. The leading particle positive excess dominates over K^+K^- pair production, unlike in the pion case. Again we parameterize the dependency in $\log_{10}E_\mu$ from Equation 16 such that

$$(1 - r^K(E_\mu)/2.61) = 2/3 \times (1 - r^\pi(E_\mu)/1.25) \quad (21)$$

The effect on the muon charge ratio due to the heavy ions requires that the pion and kaon fractions be modified as follows:

$$f_\pi^*(E_\mu) = 1/(1 + 1/r_\pi \times r^\pi(E_\mu)) \quad (22)$$

$$f_K^*(E_\mu) = 1/(1 + 1/r_K \times r^K(E_\mu)) \quad (23)$$

Including these contributions from heavy primaries does have an impact on the calculation of parameters of the pika model. The charge ratio no longer depends just upon $E_\mu \cos \theta$. While this effect is small it is certainly present and can be accounted for in modeling. Figure 19 shows the effect of the heavy primaries on the two parameters of the pika model. The fit to the data is almost indistinguishable from the previous fit. Note that an increasing heavy primary fraction at high energy will decrease the charge ratio, so to fit to the high MINOS points, a larger value of r_K is required. It is clear that simulations of the muon charge ratio need to include the possible different energy dependence of heavy primaries.

We repeat that the choice of spectral index in Table 2 is to illustrate the size of a possible effect. If it turns out that the spectral index is independent of chemical composition, the effect described in this section will not exist.

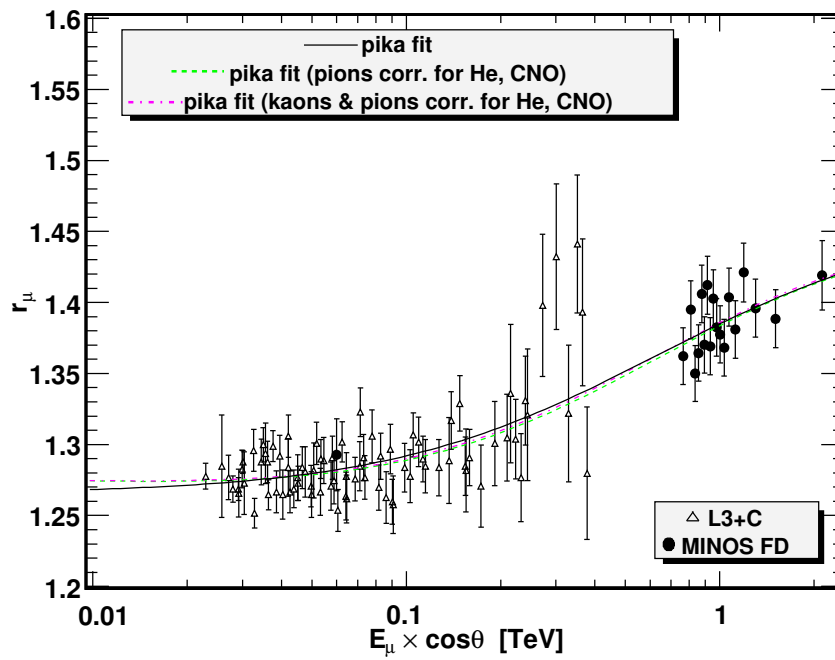


Figure 19: Fit to the meson charge ratios modifying the pika model with the energy dependence of Helium and CNO production.

8. Discussion

We have considered the change in the charge ratio from the fact that μ^+ lose slightly more energy than μ^- while penetrating the overburden of an underground detector, both for ionization and catastrophic energy loss. For catastrophic energy loss, the effect is negligible, even for the small errors in MINOS. For ionization, we have calculated that the 0.15% difference in energy loss leads to a 0.6% difference in measured r_μ at 2000 mwe. This effect was mentioned in Reference [1] but not used to correct the reported charge ratio there. In this paper, we correct the MINOS data to slightly higher values. For the Far Detector data reported in Reference [1], this is a + 0.6% correction, and for the near detector at 250 mwe the correction is +0.37%. We estimate a +0.28% correction for L3+C.

The central result of this paper is the development and application of Equation 13 and the consequent relationship of r_μ to r_π and r_K . We have used that equation to study its consistency with several simulations, and to make fits to data. In Table 3, we show the fits for our parameters to the simulations. We also show the fits to the data reported in References [1], [2], [9] and [36].

		r_K	r_π
Simulations	Lipari	2.87	1.25
	CORT	2.39	1.26
	Honda	1.63	1.28
	Gaisser [4]	3.2	1.4
	Agrawal [37]	2.92	1.35
Data fits	MINOS and L3	2.34 ± 0.07	1.227 ± 0.003
	MINOS N+F	2.26 ± 0.29	1.241 ± 0.035
	Helium γ 2.74 \rightarrow 2.64	2.73 ± 0.09	1.234 ± 0.003

Table 3: Pika fits to r_K and r_π for simulations and data.

We have shown the importance of using $E_\mu^{surface} \cos \theta$ (instead of just energy) in the analysis of the atmospheric muon charge ratio for energies above 10 GeV. Understanding of the muon charge ratio would benefit if future experiments and theory simulations would provide results using $E_\mu^{surface} \cos \theta$. The rise in the charge ratio, which occurs between the π and K critical energies of 115 GeV and 850 GeV, can be used to determine the meson

charge ratios K^+/K^- and π^+/π^- . This is an important new method for obtaining information on these ratios.

We further showed the effect on the charge ratio assuming that there is a spectral index for cosmic ray Helium nuclei which is different than the spectral index for protons. Using an index of 2.74 (2.64) for H (He), we get a change in r_K from 2.3 to 2.7 compared to an analysis where the spectral indices were the same.

Both the data and the simulations seem to have consistent values for r_π . A general feature of our analysis is that the new MINOS data by themselves suggest a lower value of r_K than is used in many of the simulations. However, it is important to note that the systematic effects considered in this paper, which include remaining errors from randomization, corrections for differences in dE/dx for μ^+ and μ^- and a possible lower spectral index for Helium, would all tend to raise the fitted values of r_K .

Several effects which have not been explicitly considered here are expected to be small. These include the production of muons from charm and other heavy particles, components of the cosmic rays heavier than Helium and possible differences in their spectra, and a variety of scaling violations which would have the effect of making f_π and f_K energy dependent. These effects need full simulations to evaluate fully; but it is important that the full simulations yield the experimentally measured average values of these parameters. In that context, the analysis presented in this paper can be useful.

9. Summary

We have reviewed several factors which affect the measurement and interpretation of the muon charge ratio r_μ deep underground. While many quantities in cosmic ray physics are difficult to measure precisely, r_μ has been measured in MINOS with a statistical accuracy better than 0.3%. In order to take advantage of this high precision, an experiment must control systematic errors to a comparable level, which is challenging. We pointed out two kinds of systematic error, those which might bias the measurement of r_μ , and those which randomize (and hence lower the measured value from the true value). Bias errors can be canceled to high precision by using data with both magnetic field polarities and Equation 5, and the success of this cancellation can be checked for consistency. Randomization errors, on the other hand, require severe cuts that affect the statistical precision. Variables

which may be related to randomization effects can be identified and used to cut out data which may be affected by randomization. However, there is no independent way to determine if all such effects have been eliminated. The possibility exists that the true values of the charge ratio are higher than those that have been reported.

The MDM is an important parameter for an experiment with a magnet. It affects both the calculation of the systematic error and the energy resolution, and also directly limits the range of detected muon energies useful for measuring r_μ and $E_\mu^{surface} \cos \theta$.

We note that to fully explore the rise in the charge ratio observed by MINOS, there is a need for additional precise ratio data in the $E_\mu^{surface} \cos \theta$ ranges of 0.2-0.8 TeV, and above 3 TeV.

10. Acknowledgments

This work was supported by the U.S. Department of Energy and Benedictine University. We would like to thank V. Naumov for introducing us to the issues involved in the predicted rise of the charge ratio. We thank Tom Gaisser, Morihiko Honda, Paolo Lipari and Teresa Montaruli for discussions on the ratio simulations. We acknowledge the help and insight of Giles Barr, Thomas Fields, Jeff de Jong and Alec Habig. We are grateful to Geoff Bodwin and Stanley Wojcicki for their contributions in understanding issues involving energy loss. We thank Eric Beall, Gavril Giurgiu, Eric Grashorn, Andrew Hoffman, Sue Kasahara, Stuart Mufson, Brian Rebel and Keith Ruddick for their many contributions. And the support of the entire MINOS collaboration has been invaluable.

References

- [1] P. Adamson et al., "Measurement of the Atmospheric Muon Charge Ratio at TeV energies with MINOS", Phys. Rev. D76 052003 (2007).
- [2] P. Adamson et al., to be published. Also J.K. De Jong for MINOS, HE2.1(627), Proceedings of the 30th International Cosmic Ray Conference, Merida Mexico, 2007.
- [3] G. Fiorentini, V.A. Naumov and F.L. Billante, Phys. Lett. B **510**, 173 (2001). V. Naumov, private communication.

- [4] T. Gaisser, “Cosmic Rays and Particle Physics”, Cambridge University Press, 1990.
- [5] Zatsepin and Kuzmin, Soviet Physics JETP volume 12, June 1961.
- [6] T.Hebbeker and C. Timmermans, Astropart. Phys. 18 107 (2002).
- [7] D. Zimmermann, et al., Nuclear Inst. and Methods in Physics Research A, 141, 525 (2004).
- [8] J. M. Baxendale, C. J. Hume, and M.G.Thompson, J. Phys G 1, 781 (1975).
- [9] P. Achard et al., Phys. Lett. B 598, 15 (2004).
- [10] S. Matsuno et al., Phys. Rev. D 29, 1 (1984).
- [11] B. C. Rastin, J. Phys. G 1629 10 (1984).
- [12] P.J. Hayman et al., Nature 195 166 (1962).
- [13] I. C. Appleton, M.T. Hogue, and B.C. Rastin, Nucl. Phys. B 26 365 (1971).
- [14] B. C. Nandi, M.S. Sinha, Nucl. Phys. B 40 289 (1972).
- [15] J. Kremer et al., Phys. Rev. Lett. 83 4241 (1999).
- [16] T. H. Burnett et al., Phys. Rev. Lett. 30 937 (1973).
- [17] M. Goodman for MINOS, HE2.1 (635), Proceedings of the 30th International Cosmic Ray Conference, Merida Mexico, 2007.
- [18] D.E.Groom et al., “Muon stopping-power and range tables,” Atomic Data and Nuclear Data Tables, 78, 183 (2001).
- [19] C. Amsler et al., Phys. Lett. B667 1-5(200); standard rock is described in section 24.4 on page 256.
- [20] Letter from E. Fermi to W. Barkas (1953).
- [21] J. Jackson and R. McCarthy, Phys. Rev. **B 6** 4131 (1972).
- [22] F. Smith, W. Birnbaum and W. Barkas, Phys. Rev. **91**, 765 (1953).

- [23] W. Barkas, W. Birnbaum and F. Smith, Phys. Rev. **101**, 778 (1956).
- [24] M. Agnello et al., Phys. Rev. Lett. **74** 371 (1995).
- [25] A. Clark et al., Phys. Lett. **41b** 229 (1972).
- [26] J. D. Jackson, Phys. Rev. **D 59**, 017301 (1998).
- [27] J. Reichenbacher, HE2.1(668), Proceedings of the 30th International Cosmic Ray Conference, Merida Mexico, 2007.
- [28] V. N. Baier and V. N. Katkov, Sov. Phys. Dokl. **21** 150 (1976).
- [29] R. N. Lee et al., Phys. Rev. A **69** 022708 (2004).
- [30] J. D. Jackson, private communication to S. Wojcicki, Nov. 4, 2005.
- [31] J. Reichenbacher, HE2.1(707) Proceedings of the 30th International Cosmic Ray Conference, Merida Mexico, 2007.
- [32] J. De Jong for MINOS, HE2.1 (697), Proceedings of the 30th International Cosmic Ray Conference, Merida Mexico, 2007.
- [33] P. Lipari, Astroparticle Physics 1 195 (1993).
- [34] M. Honda, et al., Phys. Rev. D 52 4985 (1995) and T. Sanuki et al., 29th International Cosmic Ray Conference 9 139 (2005).
- [35] Gaisser and M. Honda, arXiv:hep-ph/0203272 v2 (30 March 2002).
- [36] P. Schreiner and M. Goodman for the MINOS collaboration, HE2.1 (630), Proceedings of the 30th International Cosmic Ray Conference, Merida Mexico, 2007.
- [37] Vivek Agrawal, T.K. Gaisser, Paolo Lipari, and Todor Stanev, Phys. Rev. D 53, 1314 (1996).